Group behavior of nanoparticles translocating multiple nanopores

*Chenyu Wen,† Shuangshuang Zeng†, Zhen Zhang,† Shi-Li Zhang†**

† Division of Solid-State Electronics, The Ångström Laboratory, Uppsala University, SE-751 21 Uppsala, Sweden

Abstract: Nanopores have been implemented as nano-sensors for DNA sequencing, biomolecule inspection, chemical analysis, nanoparticle detection, *etc*. For high-throughput and parallelized measurement using nanopore arrays, individual addressability has been a crucial technological solution in order to enable scrutiny of signals generated at each and every nanopore. Here, an alternative pathway of employing arrayed nanopores to perform sensor functions is investigated by examining the group behavior of nanoparticles translocating multiple nanopores. As no individual addressability is required, fabrication of nanopore devices along with microfluidic cells and readout circuits can be greatly simplified. Experimentally, arrays of less than 10 pores are shown to be capable of analyzing translocating nanoparticles with a good signal-to-noise margin. According to theoretical predictions, more pores (than 10) per array can perform high-fidelity analysis if the noise level of the measurement system can be better controlled. More pores per array would also allow for faster measurement at lower concentration because of larger capture cross-sections for target nanoparticles. By experimentally varying the number of pores, the concentration of nanoparticles or the applied bias voltage across the nanopores, we have identified the basic characteristics of this multi-event process. By characterizing average pore current and associated standard deviation during translocation and by performing physical modeling and extensive numerical simulations, we have shown the possibility of determining the size and concentration of two kinds of translocating nanoparticles over four orders of magnitude in concentration. Hence, we have demonstrated the potential and versatility of the multiple-nanopore approach for high-throughput nanoparticle detection.

Keywords: Nanopore sensor, multiple nanopores, nanoparticles, group behavior, translocation, ionic current

Nanopore technology, with a focus on correlating the detected pulses of ionic current through a nanopore to the properties of translocating molecules, has been widely studied for DNA sequencing[1,2], biomolecule inspection[3–6], chemical molecule/ion sensing[7–9], and nanoparticle detection[10–12]. With the development of micro/nano-fabrication technologies[13–15], smaller-size pores can be drilled in thinner membranes of solid-state materials[16,17] and the sensing resolution is consequently enhanced. As another family of nanopores, biological pores naturally 1-4 nm in diameter, such as α-hemolysin (α-HL)[18], Mycobacterium smegmatis protein A[19], Phi29 connector[20], Aerolysin[21], Cytolysin A[22], Outer Membrane Protein G[23], *etc*., have been explored for biosensing applications especially in DNA sequencing. In order to improve the sensing performance, efforts have been pursued with respect to novel device structures such as field-effect transistor (FET)-nanopore devices[24,25], pore-cavity-pore device[26], and zero-depth nanopore[27], to new detection method such as plasmonic nanopore[28] and scattering nanopore[29], as well as to unconventional signal pick-up circuits and data processing algorithms[30–32]. These attempts have an implicit focus on boosting the capability of single nanopores in sensing. In contrast, simultaneous translocation of a multitude of nanopores or nano-channels by a large number of nanoparticles for high-throughput and low-cost parallelized sensing has received much less attention.

Several fabrication methods are available for production of solid-state nanopore arrays, *e.g.*, photolithography with silicon on insulator (SOI) wafers[33], electron beam lithography[34], lift-off by polystyrene[35], and controlled breakdown[36]. Moreover, protein nanopores, *e.g.*, α-HL, can self-assemble on a lipid membrane to form multiple nano-channels[37]. However, the signal readout solutions developed for nanopore arrays are mainly based on individual addressability employing either multiple electronic amplifier cells[31,38,39] (including MinION sequencer[2]), optical fluorescence microscopy[40,41], or mechanically moving and contacting stage[42]. Individual addressability implies that events at each and every nanopore of a nanopore array can be independently captured and analyzed, since the nanopores are accessed through separate electrodes, microfluidic cells, and readout electronics. It sets high engineering demands on the integration density, particularly by the resource-demanding microfluidic cells. To offset this challenge, it is valuable to explore the possibility of accurately interpreting the measured ionic current that represents a superposition of the ionic

currents from a multitude of nanopores. As shown is Figure 1(a), the output ionic current is contributed by all the pores in the membrane simultaneously. The stochastic nature of such an output ionic current has been considered[43] in the similar vein to a multi-channel patch in cell biology technology[44]. However, these previous studies focus on signals consisting of distinguishable individual translocation peaks or steps when the translocation events occurring at each pore are of relatively low probability[37,43,45–47]. This is graphically presented as case I in Figure 1(b). If the number of the pores is larger and/or the translocations are more frequent, the blockage events from different pores can severely overlap thereby making the output signal indiscernible for the established tools based on the stochastic process theory. This situation is shown as case II in Figure 1(b).

In this study, group translocation is investigated by examining how the ionic current is varied with increasing the number of nanopores from 1 to 100. Clear trends in average ionic current (I_{ave}) and its standard deviation (STD) are observed when changing the concentration of translocating nanoparticles and bias voltage. An analytical model is established to describe the characteristic behaviors of ionic current when numerous nanoparticles simultaneously and randomly translocate multiple nanopores. By virtue of statistics, this model captures the characteristics of group translocation in form of I_{ave}, STD and power spectrum density (PSD). An excellent agreement of the model prediction with the experiment confirms the validity of the model. Further validated by numerical simulation, the model is used for additional translocation scenarios to project the capability and potential of multiple-nanopore devices for parallelized nanoparticle sensing based on analysis of I_{ave} and STD. Finally, employing arrayed nanopores is obviously advantageous over using a single large pore of equivalent total opening area, because the array exhibits a much higher signal-to-noise ratio (SNR) and larger capture cross-section for the translocating nanoparticles. As a result, the array can detect particles at lower concentration within shorter time interval (Supporting Figure S1).

Results and discussion

Ionic current for translocation with different number of pores

Ionic currents for the translocation of 30 nM SiO_2 nanoparticles of 160 nm in diameter, with a spread of $\pm$22 nm determined by means of dynamic light scattering (DLS), through

SiN_x pores of 400 nm in diameter were measured in a KCl solution with the resistivity of 2.8 Ωm and at 200 mV bias voltage. For this set of experiment, the number of pores *N* on a device was successively increased from 1 to 10. The distance between adjacent pores in the array was larger than 2 μm in all devices, which, according to the COMSOL simulation, was sufficient for the 400-nm pores to form an identical distribution of electric field regardless of their position in the membrane (see Supporting Figure S1). By increasing the number of pores, current spikes generated by individual translocation events, shown as current traces in Figure 2(a), become increasingly difficult to separate and distinguish. Note that "spikes" and "peaks" are used in this work to describe sharp valleys in ionic current observed experimentally and in theoretical calculations. For the device with a single pore, there are numerous spikes in the 1-s-current segment shown in Figure 2(a). Three of the spikes are relatively high in amplitude and they could result from the translocation of multiple stuck-together particles or from nanoparticles briefly adhered around the nanopore. However, the spikes become hardly discernible when the number of pores is larger than five. In order to show the details of the waveform, the traces are displayed in Figure 2(a) after subtracting from their respective average value. The superposition of the individual ionic currents makes the (total) output current fluctuate severely.

The PSD curves of these current traces were calculated by means of Fast Fourier Transform (average of the PSD of six 1-s-current segments) and shown in Figure 2(b). It is obvious from the PSD curves that the current fluctuation increases with increasing the number of pores, which is consistent with the observation in Figure 2(a). The results of I_{ave} and STD for the different devices are depicted in Figure 2(c) and (d), respectively. For each device with a definite number of pores, six 1-s-current segments are selected arbitrarily from the trace records. The squares represent the mean values with their STD to define the error bars, while the solid lines are the results of our analytical model that will be discussed in a separate section below. While I_{ave} increase linearly with increasing the number of pores, the variation of STD with the number of pores follows a square root law. The agreement between experiment and model for both I_{ave} and STD is good. It should be mentioned that the uncertainty of STD (shown by the error bars) is smaller than the spread of nanoparticles size. This observation indicates that the discreteness of nanoparticle size did not cause a major

effects in our measurements.

Both the background noise from the pores themselves along with the electrolyte system they are in and the current fluctuation generated by the stochastic translocations are increased by further increasing the number of pores per device. The former increases faster than the latter and becomes totally dominant in the low-frequency domain of PSD[48] (see more in the "potential applications and signal-noise properties" section below). Under this condition, the information about translocation is hidden in the background noise and the device loses its function as a sensor. In our experiment, a significant difference in PSD between the open pore case without translocating nanoparticle and the nanoparticle translocation case is not observed when the number of pores is above 30 (see Supporting Figure S2).

Group behavior of five pores

Considering the noise issue, a five-pore device was chosen as an example to study the properties of group behavior of nanoparticle translocation. The traces of ionic current were retrieved at bias voltage ranging from 100 to 500 mV and with concentration of nanoparticles ranging from 0.03 to 30 nM (*i.e.*, $1.8 \cdot 10^{10}$ to $1.8 \cdot 10^{13}$ nanoparticles/ml). Both I_{ave} and STD are given in Figure 3, and as previous each data point with error bars is determined using six 1-s-current segments randomly selected from the current traces. The solid lines represent predictions of our analytical model and they are in good agreement with the experimental data. It is clear that increasing the concentration of nanoparticles leads to a decrease in I_{ave}. However, STD shows a more complex trend in Figure 3(c), first with an increase with increasing the concentration until it reaches a maximum. It then falls off at higher concentrations. This maximum appears at lower concentrations at higher bias voltages, moving from >30 nM at 100 mV to 0.1 nM at 500 mV. This behavior indicates synergistic effects of voltage and concentration on STD, because both can enhance the capture probability of nanoparticles. When the same group of data is plotted with bias voltage as the x-axis in Figure 3(b),(d), both I_{ave} and STD increase monotonously with voltage within the studied interval. The increases coincide well with the trends predicted by the model.

Analytical model for the group behavior

It is seen from the waveform of ionic current that the randomly generated blockage spikes resemble those of random telegraph noise (RTN)[49] when nanoparticles translocate a single nanopore. The occurrence of nanopore blockage is random and governed by the Poisson process. As the schematic diagram in Figure 1(b) shows, the ionic current appears in two states with time, *i.e.*, the open pore state and the blockage state, denoted "o" and "b" in the subscript of related variables, respectively. The dwell time of these two states obey exponential distribution[49,50]. Following the expression of the PSD value of RTN[49], the PSD of the translocation waveform of ionic current can be written as

$$S(f) = \frac{4\Delta I^2}{(\tau_o + \tau_b)[(\frac{1}{\tau_o} + \frac{1}{\tau_b})^2 + (2\pi f)^2]} \quad (1)$$

where, f is frequency and ΔI is the current difference between the two states (*i.e.*, the amplitude of blockage), and τ_o and τ_b are mean dwell time in open pore state and blockage state, respectively.

For devices with multiple nanopores, the additivity for a linear system leads to the following relationship:

$$S_N(f) = \sum_{i=1}^{N} S_i(f) + \sum_{i=1, j=1, i\neq j}^{N,N} S_{i,j}(f) \quad (2)$$

where, N is the number of pores, $S_N(f)$ is the total PSD, $S_i(f)$ is PSD of the ionic current from the i^{th} pore, and $S_{i,j}(f)$ is the cross PSD of ionic current from i^{th} and j^{th} pores. A reasonable assumption for multiple nanopores is that the translocation events at different pores are independent and there is no correlation among one another. Thus, $S_{i,j}(f)$ is always equal to zero and $S_N(f)$ is simply the algebraic addition of all S_i (f). Furthermore, STD of the total current can be acquired by integrating the spectra over the entire frequency range:

$$STD = \sqrt{\int_0^\infty S_N(f)df} = \frac{\Delta I\sqrt{N\tau_o\tau_b}}{(\tau_o + \tau_b)} \quad (3)$$

It can be easily shown that STD reaches its maximum when τ_o=τ_b, and the maximum STD is equal to $\Delta I\sqrt{N}/2$ (see detailed derivations in Supporting Note 1).

On the other hand, I_{ave} can be calculated straightforwardly by averaging the current:

$$I_{ave} = I_o \tau_o + (I_o - \Delta I)\tau_b \quad (4)$$

where, I_o is the open-pore current.

The time interval between two consecutive translocation events τ_o is shown in the literature to be the reciprocal of capture probability P[51]. The latter, P, describes the probability of a nanopore capturing a nanoparticle in a unit time span. It is proportional to the concentration of nanoparticles and exponentially proportional to the bias voltage[50–53]. The blockage duration τ_b is set to constant in the model fitting, since τ_b has a much weaker dependence on the bias voltage than τ_o does[52,53] (see Supporting Note 2). Specifically, τ_b = 2 ms is chosen by referring to the statistical results for the experiment of 160 nm SiO_2 nanoparticles translocating a single 400 nm pore. In the model, I_o and ΔI are determined by the size of nanopores and nanoparticles[54]:

$$I_0 = UG = \frac{U\pi d_p^2}{\rho L_{eff}} \quad (5)$$

where, G is the nanopore conductance, U is the bias voltage, ρ is resistivity of the electrolyte in the pore, L_{eff} is the effective transport length of the nanopore along which the highest electric field is measured[54], and d_p is diameter of nanopore. If a nanoparticle with diameter of d_{NP} translocates the nanopore, the blockage current level can be simply determined by the ratio in cross-section area of the nanoparticle to the nanopore[55]:

$$\Delta I = I_0 \frac{d_{NP}^2}{d_p^2} \quad (6)$$

By specifying the bias voltage, nanoparticle concentration, size of nanopores, and size of nanoparticles, the four input variables, τ_0, τ_b, I_o, and ΔI, can be determined. Then, I_{ave}, STD, and SPD can be calculated according to the model. The good agreement between model and experiment verifies the validity and efficiency of the model. More importantly, it indicates that the model captures the physics process and represents the essential properties of the group behavior of multiple nanopores translocated by numerous nanopores simultaneously and randomly.

Simulation of ionic current

A simulation platform is developed and implemented on MATLAB to perform theoretical experiments in order to explore additional features of the group behavior. The simulation is based on stochastic processes and applied by the following steps. 1) A time step Δt, *i.e.*, sampling rate, is first specified in the simulation. 2) A state of either "open pore" (o) or "blockage" (b) is randomly generated for each pore at each Δt according to a two-point distribution based on the capture probability P. 3) I_o is assigned for pores in state "o" and $I_b = I_o - \Delta I$ for pores in state "b". 4) The total current is calculated by summing up the individual currents from all pores. It is worth to mention that a pore cannot change to state "o" until lasting for τ_b, once it is in state "b". 5) Steps 2-4 are repeated to acquire the total current for the next time point, wherein the current trace is simulated over the time span equal to the inverse of the lowest frequency of noise PDS. 6) I_{ave}, STD, and PSD are calculated using the generated current traces in the time domain.

The simulated waveform of the output ionic current for a single pore being translocated by numerous nanoparticles shows the expected pattern of blockage spikes in Figure 4(a). The results also reproduce well the experimental observations for multiple nanopores in Figure 2(a). The PSD calculation was performed by averaging ten 1-s-current segments and the results are displayed in Figure 4(b). Overall, the simulation agrees well with the modeling. A typical Lorentzian PSD coincides excellently with the model (Eq. 1). The corresponding I_{ave} and STD as a function of number of pores are summarized in Figure 4(c). The simulation is found to agree excellently with the modeling for both I_{ave} and STD. Similarly to the experimental observations in Figure 2(c),(d), I_{ave} increases linearly with increasing the number of nanopores while STD follows a square root law, at the given bias voltage and concentration of nanoparticles.

As discussed earlier, both bias voltage and concentration of nanoparticles can affect the capture rate. Hence, both I_{ave} and STD are sensitively dependent on these parameters. As shown in Figure 4(d), I_{ave} increases continuously with bias voltage while STD firstly increases to a maximum value and then decreases at high bias voltages. The observed behavior of STD can be understood with the assistance of the model. At low bias voltages, the capture rate increases with increasing bias voltage. Yet, τ_b is still kept below τ_o. The relatively shorter τ_o pushes up the fluctuation level. However, the capture rate can reach a very large value by

further increasing the bias voltages, to the extent that τ_b becomes longer than τ_o. In this case, the shorter τ_0, the lower fluctuation level of the ionic current is. It is seen that the agreement between simulation and modeling is excellent for I_{ave}. Although the comparison is somewhat compromised for STD, it is important to note that both simulation and modeling capture the basic feature of how fluctuation evolves with bias voltage.

The variation of I_{ave} and STD as a function of the concentration of nanoparticles in Figure 4(e) shows that I_{ave} keeps decreasing with increasing the concentration of nanoparticles and this decrease becomes accelerated above 1 nM. The behavior of STD is similar to its variation with bias voltage; STD increases under the condition $\tau_o > \tau_b$ but it declines when $\tau_o < \tau_b$. While STD is characterized by a maximum when either bias voltage or concentration of nanoparticles is varied, the distinct behavior of I_{ave} with these two experimental parameters, which is consistent with the experimental observations in Figure 3(a),(b), can be useful in guiding the experimental design.

Potential applications and signal-noise properties

The potential of utilizing the group behavior of multiple nanopores to decipher the translocation properties is further explored for several application scenarios. It shows the potential to discriminate two kinds of nanoparticles of distinct diameters in dispersions and gauge their concentration ratio. The experiment data of I_{ave} and STD are shown as discrete dots in Figure 5 for various mixtures of SiO_2 nanoparticles of 20 ± 2 and 160 ± 22 nm in diameter translocating a five-pore device. An almost linear increase in I_{ave} is observed when varying the ratio of these two kinds of nanoparticles from 100% 160 nm diameter ($C_{NP1}/(C_{NP1}+C_{NP2})=0$) to 100% 20 nm diameter ($C_{NP1}/(C_{NP1}+C_{NP2})=1$). In contrast, STD, as expected, displays a bell shape with a maximum around the 50-50 mixture corresponding to the maximum chaos or current fluctuation. The corresponding simulation results shown as continuous lines in Figure 5 coincide very well with the experimental data. Moreover, by analyzing the details of I_{ave} and STD, lots of information, such as diameter and concentration of nanoparticles, become possible to be inferred (see Supporting Figure S4 and Supporting Table S1).

Theoretically, when a device with a larger number of pores is employed with a higher

bias voltage, more significant changes in I_{ave} and larger STD (fluctuations), both indicating stronger signals, are obtained. However, in practice, some subtle details can impede the signal boost, in particular a rapid growth of noise level and a saturation of capture rate. For low-frequency noise, three components need to be considered[48,56]: thermal noise, flicker noise and electrode noise from the interface of Ag/AgCl electrode to the electrolyte. With the increase of number of nanopores, the power of thermal noise and flicker noise increase linearly at the same speed of signal enhancement[57]. Hence, SNR will not be worsened. However, the electrode noise component increases at a higher pace since it grows in a quadratic fashion with the number of nanopores[48]. Consequently, the noise level will override the signal beyond a certain number of nanopores (see detailed derivations in Supporting Note 3).

In the model, an important assumption is the independence of the translocation events, including the independence in space (*i.e.*, the events at different pores are not correlated) and time (*i.e.*, one event does not influence the next one at the same pore). Thus, this stochastic process is stationary and ergodic, which is a prerequisite for the Lorentzian PSD of the ionic current of the nanopore being translocated by nanoparticles. However, if the concentration of nanoparticles is large and/or the bias voltage is high, the previous translocation event may retard the following one and they are not independent any more. Moreover, the nanoparticles may adhere on the mouth/wall of a pore, become conjugated and partially clog the pore (Supporting Figure S3). Under such circumstances, the translocation event at a chosen pore is not entirely isolated from those at adjacent pores.

In experiment, additional factors could induce uncertainties and lead to results departing from the model predications. Size distribution of the nanoparticles can introduce additional fluctuations in amplitude and duration of the translocation current spikes. Consequently, it can inevitably complicate STD of multiple-pore devices. Furthermore, inadequate cleaning and incomplete wetting of nanopore could mess the random translocation and induce an unstable open pore current, which can lead to an increase of the background noise. Keeping raising the concentration of nanoparticles and bias voltage can lead to saturation of the capture rate. In other words, the rate limiting step is the translocation speed not the capture rate. In this case, I_{ave} and STD become unconnected to the concentration of nanoparticles and the sensing

function is defeated. Considering this extreme situation, the detection limit of nanoparticle concentration can be worsened by increasing number of nanopores (see detailed discussions in Supporting Note 3).

Conclusions

The present work attempts to establish the foundation for the group behavior of numerous nanoparticles translocating multiple nanopores simultaneously and randomly. Higher pore number promises faster measurement at lower concentration of nanoparticles, as a result of larger capture cross-sections for the target nanoparticles. The systematic study presented in this work reveals that I_{ave} and STD are two important output signals containing critical information of the translocation process. By increasing the number of nanopores, both I_{ave} and STD increase monotonously. However, STD displays a maximum when either the concentration of nanoparticles or the bias voltage is raised, while the monotonous variation of I_{ave} with these two parameters remains. A simple yet accurate analytical model has been established to predict the group behavior. The predictions are found to coincide well with the experimental results. Experimentally, several parameters, including bias voltage, nanoparticle concentration, distance between adjacent pores in the membrane, and number of nanopores, should be carefully varied in order to render the individual translocation events to be independent. Additionally, controlling noise and avoiding adsorption of particles on the mouth/wall of nanopores are prerequisites to increase the number of pores and boost the signal to noise ratio. Moreover, a simulation platform has also been implemented on MATLAB and its validity is confirmed by comparing with the model. The simulation is used to perform theoretical experiments and the results are in good agreement with the model calculation. By analyzing I_{ave} and STD, the multiple-nanopore technology can be employed to determine the concentration, size, and constituents of nanoparticle samples. Furthermore, more sophisticated analyses of the group behavior with the assistance of advanced mathematical, statistical, and algorithmic models and tools can help reveal more subtle information and develop wider practical applications regarding the nanoparticle translocation of multiple nanopores.

Methods

Nanopore fabrication

Electron-beam lithography (EBL) assisted by reactive ion etching (RIE) is employed to fabricate nanopores with tunable and controllable size in free-standing SiN_x membranes. Starting from a 300 μm double side polished (100) silicon wafer with a 50 nm thick SiO_2 and a 20 nm thick low-stress SiN_x membrane deposited by means of low pressure chemical vapor deposition, nanopores were patterned on the front side with EBL and then transferred into the SiN_x membrane by RIE. Next, a 150 μm window was opened on the rear side of the wafer using photolithography and RIE. Finally, deep RIE and KOH etching were carried out to strip off the thick silicon substrate layer through the rare-side opening to reach the 50-nm thick SiO_2 on the front side. This oxide was then stripped off in buffered hydrofluoric acid (BHF). Therefore, nanopores were created in the free-standing SiN_x membrane on the front side of the wafer. The SEM images of a nanopore array are displayed in Supporting Figure S6, showing a good uniformity of the pore size.

Translocation experiment and measurement

The device containing multiple nanopores was sandwiched by a custom-made polymethyl methacrylate (PMMA) flow cell between two silicone O-rings (8 mm in diameter); two compartments for KCl solution were separated by the device and the only path of the ionic current was through the nanopore. The resistivity of the KCl solution is measured using a conductivity meter (Lab 945, Xylem Analytics Germany Sales GmbH & Co. KG) .In the experiment, various concentrations of 160±22 nm and/or 20±2 nm silica particles dispersed in KCl solution could be added in both chambers. The diameter and its distribution are characterized by means of DSL (Zetasizer Nano Z, UK). In order to enhance the driving force on the nanoparticles, the silica particle dispersions were tuned to pH 10 by adding KOH solution so as to make the surface of the particles carry a relatively large density of negative charge. The nanopore chips were carefully cleaned in oxygen plasma at 1000 W for 20 min, followed by immersion in a piranha solution with H_2SO_4:H_2O=3:1 (volume ratio) for 30 min, and finally rinsed by deionized water prior to the measurement. A pair of Ag/AgCl electrodes (2 mm in diameter, Warner Instruments, LLC.) was used to apply voltage and measure ionic

current. The current was measured with a patch clamp amplifier (Axopatch 200B, Molecular Device Inc.), digitalized by Axon Digidata 1550A (Molecular Device LLC.), and recorded by the software Axon pCLAMP 10 (Molecular Device LLC.). Particle translocation was detected at 10 kHz sampling frequency with a 1 kHz 4-pole Bessel low-pass filter. The whole setup was placed inside a Faraday cage to shield from electromagnetic noise.

ASSOCIATED CONTENT

Supporting Information

The Supporting Information is available free of charge on the ACS Publications website at DOI: XXXXXXXX.

Electric field distribution of nanopore arrays; PSD of current from 30 and 100 pores with the translocation of nanoparticles with different concentrations; Optical microscope images of 100 SiN_x nanopores after the translocation of 30 nM SiO_2 nanoparticles; Modeling and simulation of I_{ave} and STD for a system with 100 nanopores; STD by the model prediction as a function of number and concentration of nanoparticles; Scanning electron microscope images of a 10x10 nanopore array in SiN_x membrane; Influence of experimental conditions on translocation parameters. Derivation of the maximum value of STD; Dependence of τ_o and τ_b on bias voltage; Properties of signal and noise in the multiple nanopore device (PDF)

AUTHOR INFORMATION

Corresponding Author

*E-mail: shili.zhang@angstrom.uu.se

Notes

The authors declare no competing financial interests.

ACKNOWLEDGMENT

The authors would like to thank Dr. Ralph Scheicher and Shiyu Li for fruitful discussions. This work was financially supported by the Swedish Research Council (621-2014-6300) and Stiftelsen Olle Engkvist Byggmästare (2016/39).

References

(1) Laszlo, A. H.; Derrington, I. M.; Ross, B. C.; Brinkerhoff, H.; Adey, A.; Nova, I. C.; Craig, J. M.; Langford, K. W.; Samson, J. M.; Daza, R.; et al. Decoding Long Nanopore Sequencing Reads of Natural DNA. *Nat. Biotechnol.* **2014**, *32* (8), 829–833.

(2) Jain, M.; Fiddes, I. T.; Miga, K. H.; Olsen, H. E.; Paten, B.; Akeson, M. Improved Data Analysis for the MinION Nanopore Sequencer. *Nat. Methods* **2015**, *12* (4), 351–356.

(3) Xi, D.; Shang, J.; Fan, E.; You, J.; Zhang, S.; Wang, H. Nanopore-Based Selective Discrimination of MicroRNAs with Single-Nucleotide Difference Using Locked Nucleic Acid-Modified Probes. *Anal. Chem.* **2016**, *88* (21), 10540–10546.

(4) Siwy, Z.; Trofin, L.; Kohli, P.; Baker, L. A.; Trautmann, C.; Martin, C. R. Protein Biosensors Based on Biofunctionalized Conical Gold Nanotubes. *J. Am. Chem. Soc.* **2005**, *127* (14), 5000–5001.

(5) Wei, R.; Gatterdam, V.; Wieneke, R.; Tampé, R.; Rant, U. Stochastic Sensing of Proteins with Receptor-Modified Solid-State Nanopores. *Nat. Nanotechnol.* **2012**, *7* (4), 257–263.

(6) Lin, Y.; Shi, X.; Liu, S.-C.; Ying, Y.-L.; Li, Q.; Gao, R.; Fathi, F.; Long, Y.-T.; Tian, H. Characterization of DNA Duplex Unzipping through a Sub-2 Nm Solid-State Nanopore. *Chem. Commun.* **2017**, *53* (25), 3539–3542.

(7) Wu, H.-C.; Astier, Y.; Maglia, G.; Mikhailova, E.; Bayley, H. Protein Nanopores with Covalently Attached Molecular Adapters. *J. Am. Chem. Soc.* **2007**, *129* (51), 16142–16148.

(8) Hou, X.; Guo, W.; Xia, F.; Nie, F.-Q.; Dong, H.; Tian, Y.; Wen, L.; Wang, L.; Cao, L.; Yang, Y.; et al. A Biomimetic Potassium Responsive Nanochannel: G-Quadruplex DNA Conformational Switching in a Synthetic Nanopore. *J. Am. Chem. Soc.* **2009**, *131* (22), 7800–7805.

(9) Cao, Y.; Lin, Y.; Qian, R.-C.; Ying, Y.-L.; Si, W.; Sha, J.; Chen, Y.; Long, Y.-T. Evidence of Single-Nanoparticle Translocation through a Solid-State Nanopore by Plasmon Resonance Energy Transfer. *Chem. Commun.* **2016**, *52* (30), 5230–5233.

(10) Goyal, G.; Freedman, K. J.; Kim, M. J. Gold Nanoparticle Translocation Dynamics and Electrical Detection of Single Particle Diffusion Using Solid-State Nanopores. *Anal. Chem.* **2013**, *85* (17), 8180–8187.

(11) Venta, K. E.; Zanjani, M. B.; Ye, X.; Danda, G.; Murray, C. B.; Lukes, J. R.; Drndić, M. Gold Nanorod Translocations and Charge Measurement through Solid-State Nanopores. *Nano Lett.* **2014**, *14* (9), 5358–5364.

(12) Yusko, E. C.; Bruhn, B. R.; Eggenberger, O. M.; Houghtaling, J.; Rollings, R. C.; Walsh, N. C.; Nandivada, S.; Pindrus, M.; Hall, A. R.; Sept, D.; et al. Real-Time Shape Approximation and Fingerprinting of Single Proteins Using a Nanopore. *Nat. Nanotechnol.* **2017**, *12* (4), 360–367.

(13) Li, J.; Stein, D.; McMullan, C.; Branton, D.; Aziz, M. J.; Golovchenko, J. A. Ion-Beam Sculpting at Nanometre Length Scales. *Nature* **2001**, *412* (6843), 166–169.

(14) Kim, M. J.; Wanunu, M.; Bell, D. C.; Meller, A. Rapid Fabrication of Uniformly Sized Nanopores and Nanopore Arrays for Parallel DNA Analysis. *Adv. Mater.* **2006**, *18* (23), 3149–3153.

(15) Ahmadi, A. G.; Peng, Z.; Hesketh, P. J.; Nair, S. Wafer-Scale Process for Fabricating

Arrays of Nanopore Devices. *J. MicroNanolithography MEMS MOEMS* **2010**, *9* (3), 033011.

(16) Deng, T.; Li, M.; Wang, Y.; Liu, Z. Development of Solid-State Nanopore Fabrication Technologies. *Sci. Bull.* **2015**, *60* (3), 304–319.

(17) Ying, Y.-L.; Long, Y.-T. Single-Molecule Analysis in an Electrochemical Confined Space. *Sci. China Chem.* **2017**, *60* (9), 1187–1190.

(18) Kasianowicz, J. J.; Brandin, E.; Branton, D.; Deamer, D. W. Characterization of Individual Polynucleotide Molecules Using a Membrane Channel. *Proc. Natl. Acad. Sci.* **1996**, *93* (24), 13770–13773.

(19) Derrington, I. M.; Butler, T. Z.; Collins, M. D.; Manrao, E.; Pavlenok, M.; Niederweis, M.; Gundlach, J. H. Nanopore DNA Sequencing with MspA. *Proc. Natl. Acad. Sci.* **2010**, *107* (37), 16060–16065.

(20) Wang, S.; Haque, F.; Rychahou, P. G.; Evers, B. M.; Guo, P. Engineered Nanopore of Phi29 DNA-Packaging Motor for Real-Time Detection of Single Colon Cancer Specific Antibody in Serum. *ACS Nano* **2013**, *7* (11), 9814–9822.

(21) Cao, C.; Ying, Y.-L.; Hu, Z.-L.; Liao, D.-F.; Tian, H.; Long, Y.-T. Discrimination of Oligonucleotides of Different Lengths with a Wild-Type Aerolysin Nanopore. *Nat. Nanotechnol.* **2016**, *11* (8), 713–718.

(22) Biesemans, A.; Soskine, M.; Maglia, G. A Protein Rotaxane Controls the Translocation of Proteins Across a ClyA Nanopore. *Nano Lett.* **2015**, *15* (9), 6076–6081.

(23) Fahie, M.; Chisholm, C.; Chen, M. Resolved Single-Molecule Detection of Individual Species within a Mixture of Anti-Biotin Antibodies Using an Engineered Monomeric Nanopore. *ACS Nano* **2015**, *9* (2), 1089–1098.

(24) Parkin, W. M.; Drndić, M. Signal and Noise in FET-Nanopore Devices. *ACS Sens.* **2018**.

(25) Yanagi, I.; Oura, T.; Haga, T.; Ando, M.; Yamamoto, J.; Mine, T.; Ishida, T.; Hatano, T.; Akahori, R.; Yokoi, T.; et al. A Novel Side-Gated Ultrathin-Channel Nanopore FET (SGNAFET) Sensor for Direct DNA Sequencing. In *2013 IEEE International Electron Devices Meeting*; 2013; pp 14.3.1-14.3.4.

(26) Pedone, D.; Langecker, M.; Abstreiter, G.; Rant, U. A Pore−Cavity−Pore Device to Trap and Investigate Single Nanoparticles and DNA Molecules in a Femtoliter Compartment: Confined Diffusion and Narrow Escape. *Nano Lett.* **2011**, *11* (4), 1561–1567.

(27) Arjmandi-Tash, H.; Bellunato, A.; Wen, C.; Olsthoorn, R. C.; Scheicher, R. H.; Zhang, S.-L.; Schneider, G. F. Zero-Depth Interfacial Nanopore Capillaries. *Adv. Mater.* n/a-n/a.

(28) Crick, C. R.; Albella, P.; Kim, H.-J.; Ivanov, A. P.; Kim, K.-B.; Maier, S. A.; Edel, J. B. Low-Noise Plasmonic Nanopore Biosensors for Single Molecule Detection at Elevated Temperatures. *ACS Photonics* **2017**, *4* (11), 2835–2842.

(29) Shi, X.; Gao, R.; Ying, Y.-L.; Si, W.; Chen, Y.-F.; Long, Y.-T. A Scattering Nanopore for Single Nanoentity Sensing. *ACS Sens.* **2016**, *1* (9), 1086–1090.

(30) Forstater, J. H.; Briggs, K.; Robertson, J. W. F.; Ettedgui, J.; Marie-Rose, O.; Vaz, C.; Kasianowicz, J. J.; Tabard-Cossa, V.; Balijepalli, A. MOSAIC: A Modular Single-Molecule Analysis Interface for Decoding Multistate Nanopore Data. *Anal. Chem.*

2016, *88* (23), 11900–11907.

(31) Shekar, S.; Niedzwiecki, D. J.; Chien, C.-C.; Ong, P.; Fleischer, D. A.; Lin, J.; Rosenstein, J. K.; Drndić, M.; Shepard, K. L. Measurement of DNA Translocation Dynamics in a Solid-State Nanopore at 100 Ns Temporal Resolution. *Nano Lett.* **2016**, *16* (7), 4483–4489.

(32) Gu, Z.; Ying, Y.-L.; Cao, C.; He, P.; Long, Y.-T. Accurate Data Process for Nanopore Analysis. *Anal. Chem.* **2015**, *87* (2), 907–913.

(33) Deng, T.; Wang, Y.; Chen, Q.; Chen, H.; Liu, Z. Massive Fabrication of Silicon Nanopore Arrays with Tunable Shapes. *Appl. Surf. Sci.* **2016**, *390*, 681–688.

(34) Bai, J.; Wang, D.; Nam, S.; Peng, H.; Bruce, R.; Gignac, L.; Brink, M.; Kratschmer, E.; Rossnagel, S.; Waggoner, P.; et al. Fabrication of Sub-20 Nm Nanopore Arrays in Membranes with Embedded Metal Electrodes at Wafer Scales. *Nanoscale* **2014**, *6* (15), 8900–8906.

(35) Mazzotta, F.; Höök, F.; Jonsson, M. P. High Throughput Fabrication of Plasmonic Nanostructures in Nanofluidic Pores for Biosensing Applications. *Nanotechnology* **2012**, *23* (41), 415304.

(36) Wang, Y.; Ying, C.; Zhou, W.; Vreede, L. de; Liu, Z.; Tian, J. Fabrication of Multiple Nanopores in a SiN x Membrane via Controlled Breakdown. *Sci. Rep.* **2018**, *8* (1), 1234.

(37) Ervin, E. N.; White, R. J.; White, H. S. Sensitivity and Signal Complexity as a Function of the Number of Ion Channels in a Stochastic Sensor. *Anal. Chem.* **2009**, *81* (2), 533–537.

(38) Magierowski, S.; Huang, Y.; Wang, C.; Ghafar-Zadeh, E. Nanopore-CMOS Interfaces for DNA Sequencing. *Biosensors* **2016**, *6* (3), 42.

(39) Fuller, C. W.; Kumar, S.; Porel, M.; Chien, M.; Bibillo, A.; Stranges, P. B.; Dorwart, M.; Tao, C.; Li, Z.; Guo, W.; et al. Real-Time Single-Molecule Electronic DNA Sequencing by Synthesis Using Polymer-Tagged Nucleotides on a Nanopore Array. *Proc. Natl. Acad. Sci.* **2016**, *113* (19), 5233–5238.

(40) Huang, S.; Romero-Ruiz, M.; Castell, O. K.; Bayley, H.; Wallace, M. I. High-Throughput Optical Sensing of Nucleic Acids in a Nanopore Array. *Nat. Nanotechnol.* **2015**, *10* (11), 986–991.

(41) Larkin, J.; Henley, R. Y.; Jadhav, V.; Korlach, J.; Wanunu, M. Length-Independent DNA Packing into Nanopore Zero-Mode Waveguides for Low-Input DNA Sequencing. *Nat. Nanotechnol.* **2017**, *12* (12), 1169–1175.

(42) Arcadia, C. E.; Reyes, C. C.; Rosenstein, J. K. In Situ Nanopore Fabrication and Single-Molecule Sensing with Microscale Liquid Contacts. *ACS Nano* **2017**, *11* (5), 4907–4915.

(43) Lazenby, R. A.; Macazo, F. C.; Wormsbecher, R. F.; White, R. J. Quantitative Framework for Stochastic Nanopore Sensors Using Multiple Channels. *Anal. Chem.* **2018**, *90* (1), 903–911.

(44) Glasbey, C. A.; Martin, R. J. The Distribution of Numbers of Open Channels in Multi-Channel Patches. *J. Neurosci. Methods* **1988**, *24* (3), 283–287.

(45) Csanády, L. Rapid Kinetic Analysis of Multichannel Records by a Simultaneous Fit to All Dwell-Time Histograms. *Biophys. J.* **2000**, *78* (2), 785–799.

(46) Dabrowski, A. R.; McDonald, D. Statistical Analysis of Multiple Ion Channel Data. *Ann. Stat.* **1992**, *20* (3), 1180–1202.
(47) Jackson, M. B. Stochastic Behavior of a Many-Channel Membrane System. *Biophys. J.* **1985**, *47* (2, Part 1), 129–137.
(48) Wen, C.; Zeng, S.; Arstila, K.; Sajavaara, T.; Zhu, Y.; Zhang, Z.; Zhang, S.-L. Generalized Noise Study of Solid-State Nanopores at Low Frequencies. *ACS Sens.* **2017**, *2* (2), 300–307.
(49) Simoen, E.; Kaczer, B.; Toledano-Luque, M.; Claeys, C. (Invited) Random Telegraph Noise: From a Device Physicist's Dream to a Designer's Nightmare. *ECS Trans.* **2011**, *39* (1), 3–15.
(50) Meller, A.; Branton, D. Single Molecule Measurements of DNA Transport through a Nanopore. *ELECTROPHORESIS* **2002**, *23* (16), 2583–2591.
(51) Wanunu, M. Nanopores: A Journey towards DNA Sequencing. *Phys. Life Rev.* **2012**, *9* (2), 125–158.
(52) Bacri, L.; Oukhaled, A. G.; Schiedt, B.; Patriarche, G.; Bourhis, E.; Gierak, J.; Pelta, J.; Auvray, L. Dynamics of Colloids in Single Solid-State Nanopores. *J. Phys. Chem. B* **2011**, *115* (12), 2890–2898.
(53) Cabello-Aguilar, S.; Chaaya, A. A.; Bechelany, M.; Pochat-Bohatier, C.; Balanzat, E.; Janot, J.-M.; Miele, P.; Balme, S. Dynamics of Polymer Nanoparticles through a Single Artificial Nanopore with a High-Aspect-Ratio. *Soft Matter* **2014**, *10* (42), 8413–8419.
(54) Wen, C.; Zhang, Z.; Zhang, S.-L. Physical Model for Rapid and Accurate Determination of Nanopore Size via Conductance Measurement. *ACS Sens.* **2017**, *2* (10), 1523–1530.
(55) Wen, C.; Zeng, S.; Zhang, Z.; Hjort, K.; Scheicher, R.; Zhang, S.-L. On Nanopore DNA Sequencing by Signal and Noise Analysis of Ionic Current. *Nanotechnology* **2016**, *27* (21), 215502.
(56) Balan, A.; Machielse, B.; Niedzwiecki, D.; Lin, J.; Ong, P.; Engelke, R.; Shepard, K. L.; Drndić, M. Improving Signal-to-Noise Performance for DNA Translocation in Solid-State Nanopores at MHz Bandwidths. *Nano Lett.* **2014**, *14* (12), 7215–7220.
(57) Smeets, R. M. M.; Keyser, U. F.; Dekker, N. H.; Dekker, C. Noise in Solid-State Nanopores. *Proc. Natl. Acad. Sci.* **2008**, *105* (2), 417–421.

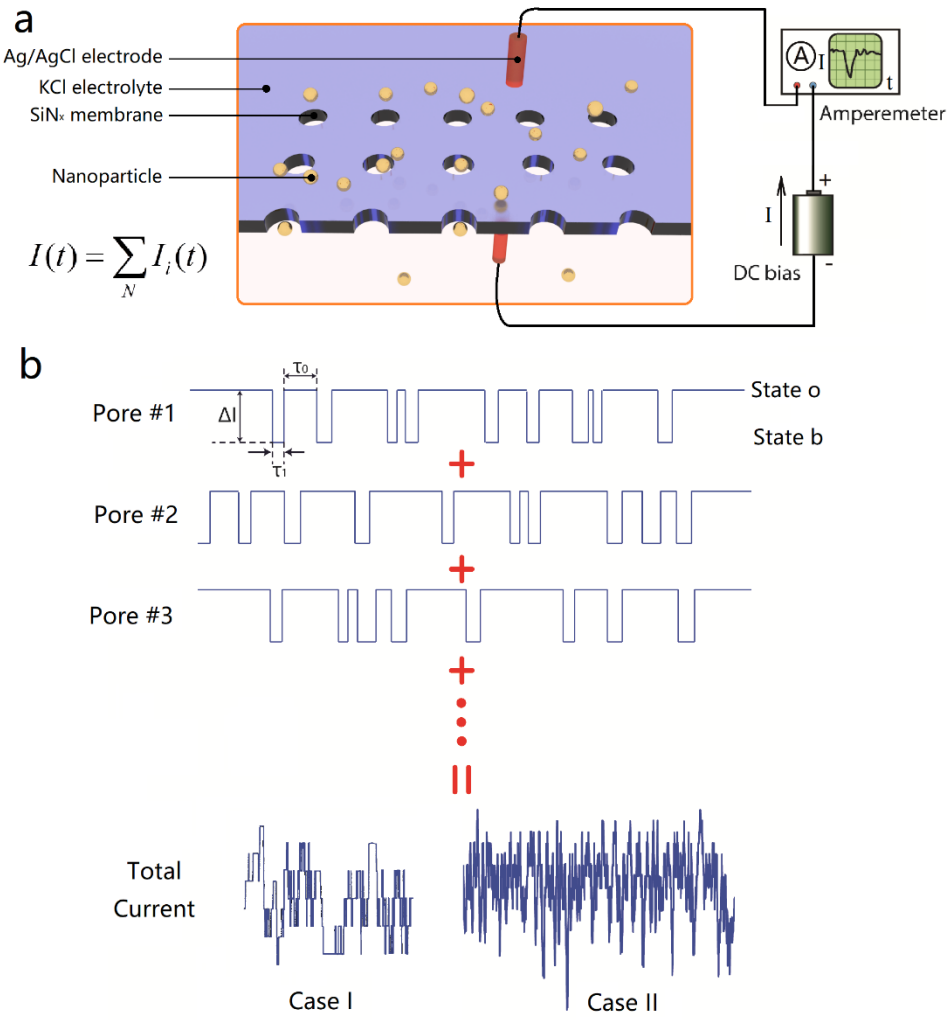

Figure 1. Device structure and signal of multiple-nanopore sensor. (a) Schematic device structure of a multiple-nanopore sensor. (b) Schematic illustrations of how sharp and clean ionic currents from three individual pores could evolve to two distinct patterns (cases) of the final output signal.

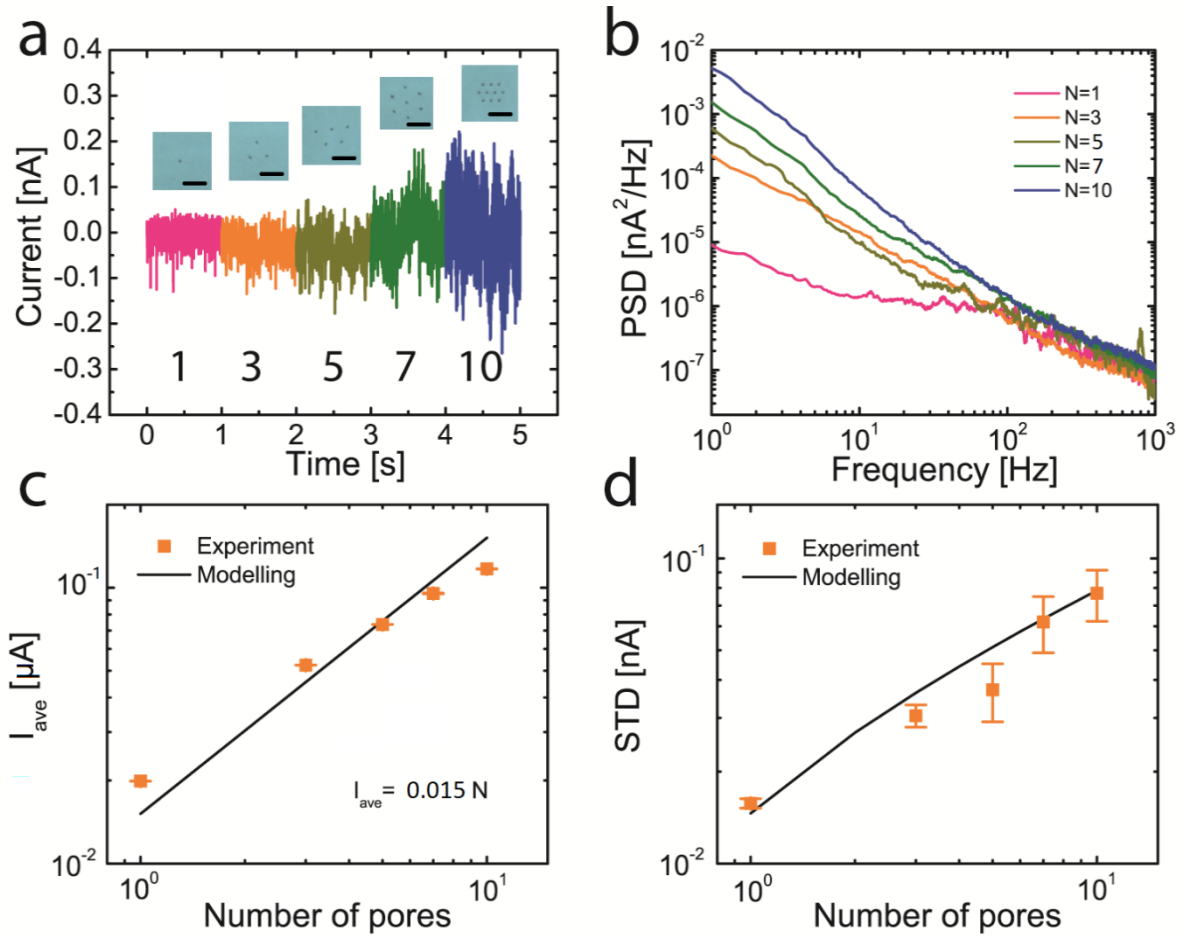

Figure 2. Experimental results of group behavior by varying the numbers of nanopores. (a) Experimentally measured ionic current traces of a single kind of nanoparticles translocating nanopores of increasing number from 1 to 10. Insets: optical microscope images of five multiple-nanopore devices. Scale bars: 5 μm. (b) PSD of ionic current for translocation with nanopores of different number of pores. (c) Variation of I_{ave} as a function of number of pores. Squares: experiment, line: model. Error bars: standard deviation of six 1-s-current segments. (d) Variation of STD as a function of number of pores following a square root law. Squares: experiment, line: model. Error bars: standard deviation of six 1-s-current segments. All the measurements in this figure were carried out with 30 nM SiO_2 nanoparticles at 200 mV bias in KCl electrolyte with the resistivity of 2.8 Ωm.

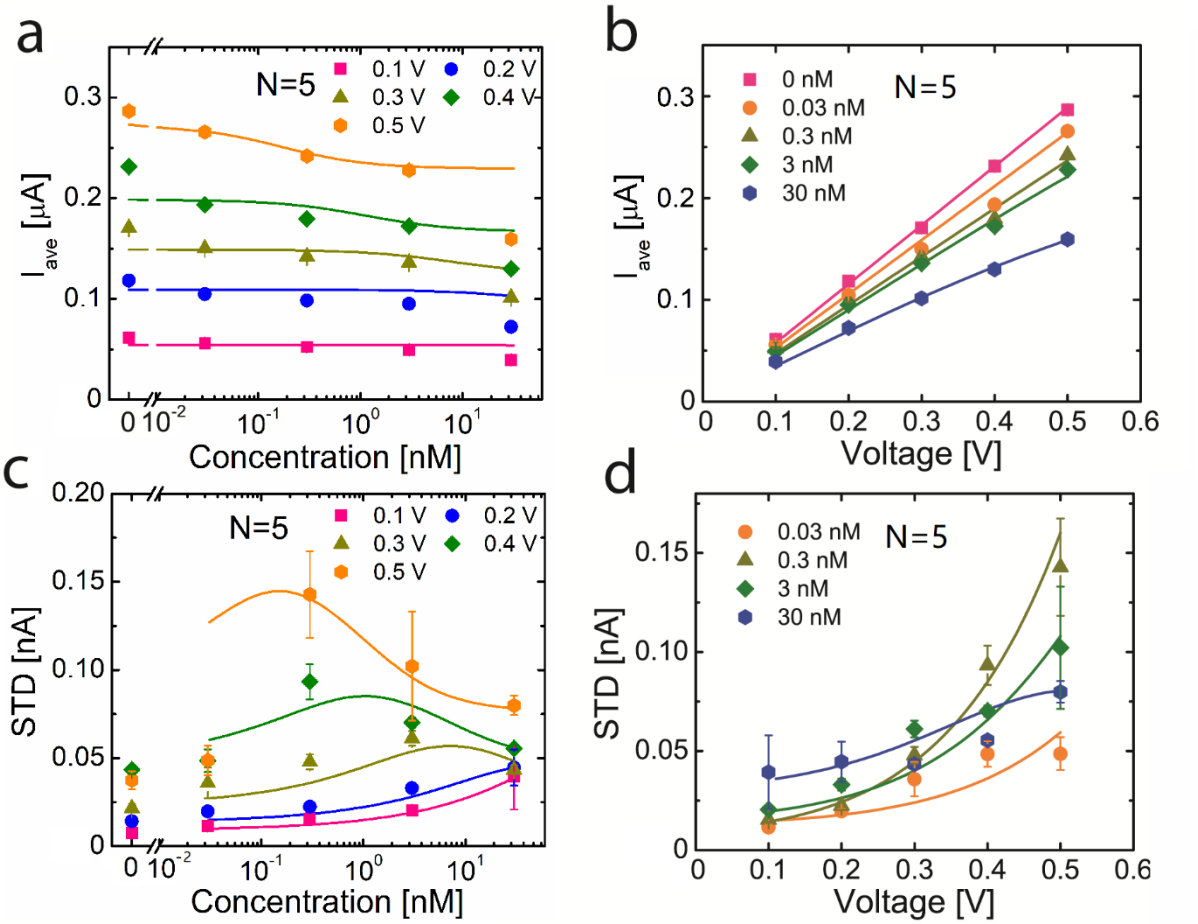

Figure 3. Comparison between experiment and model of a five-pore device. (a),(c) Variation of I_{ave} and STD with concentration of nanoparticles at different bias voltages. (b),(d) Variation of I_{ave} and STD with bias voltage at different concentration of nanoparticles. Dots: experiment, lines: model. Error bars: standard deviation of six 1-s-current segments.

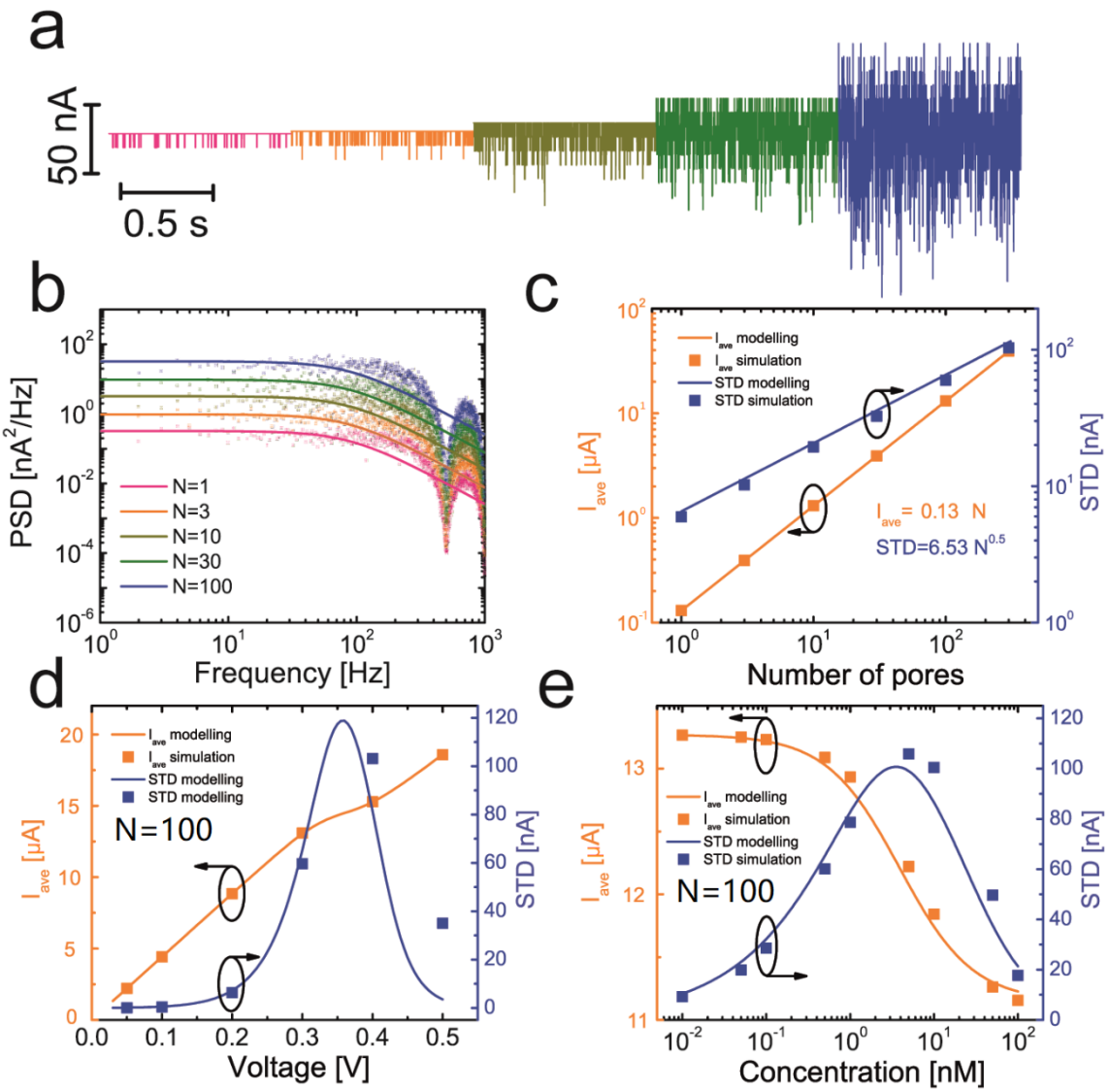

Figure 4. Modeling and simulation of group behavior. (a) Typical simulated ionic current traces of 0.5 nM nanoparticles translocating nanopores with N=1, 3, 10, 30, 100, from left to right at 300 mV bias voltage. (b) PSD with different number of pores at 300 mV bias voltage. (c) Variation of I_{ave} and STD as a function of number of pores. Concentration of nanoparticles: 0.5 nM, bias voltage: 300 mV. (d) Variation of I_{ave} and STD as a function of bias voltage for 100 nanopores with 0.5 nM nanoparticles at 300 mV bias voltage. (e) Variation of I_{ave} and STD as a function of concentration of nanoparticles for 100 nanopores at 300 mV bias voltage. Dots: simulation, solid curves: model. All the simulation and modeling were implemented for 400 nm-diameter nanopores and 160-nm diameter nanoparticles in 100 mM KCl electrolyte.

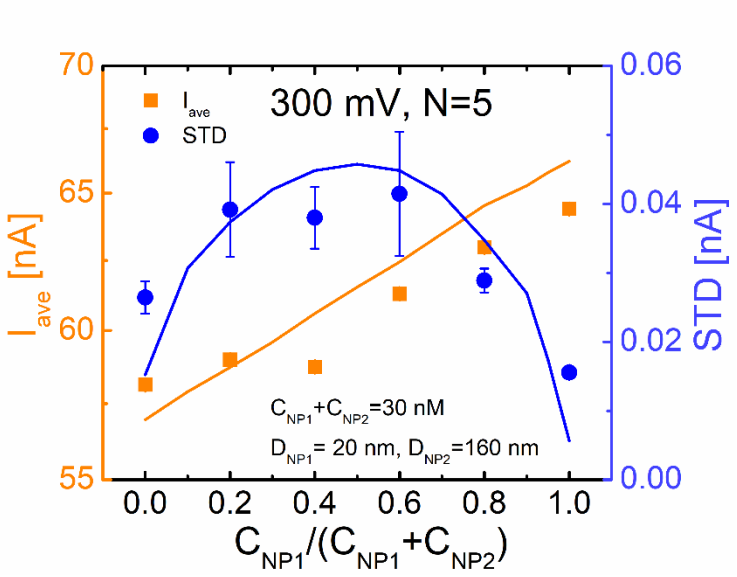

Figure 5. Experiment and simulation of I_{ave} and STD for translocation of mixture nanoparticles. Comparisons between experiment (dots) and simulation (lines) for the changes of I_{ave} and STD of current of a five-pore device, by varying the mixing ratio of type 1 SiO_2 nanoparticles (NP1, 20 nm in diameter) and type 2 SiO_2 nanoparticles (NP2, 160 nm in diameter). The total concentration of the mixture is fixed to 30 nM. The simulation and measurement were implemented at 300 mV bias and in KCl buffer with the resistivity of 6.2 Ωm. Error bars: standard deviation of six 1-s-current segments. A normalization factor was necessary to bring the simulation results to the same range of the experimental data.

TOC Figure